IEEE Access
Multidisciplinary | Rapid Review | Open Access Journal

Received February 27, 2020, accepted March 25, 2020, date of publication April 6, 2020, date of current version April 21, 2020.

Digital Object Identifier 10.1109/ACCESS.2020.2985688

Accurate Estimation of Ground Obstacle Collision Probability During ILS Approach

RYOTA MORI[1] **AND MASATO FUJITA**[2]
[1]Electronic Navigation Research Institute, Tokyo 182-0012, Japan
[2]Japan Coast Guard Academy, Hiroshima 737-0832, Japan

Corresponding author: Ryota Mori (r-mori@mpat.go.jp)

ABSTRACT This paper proposes a new high-accuracy calculation method to estimate collision probability to ground obstacles during Instrument Landing System (ILS) approach. The current collision risk model (CRM) used to evaluate the ground obstacle collision probability was developed in the 1970s. In this CRM, a shadowing technique is used to avoid over-estimation of the risk when there are multiple obstacles located close to each other. However, this shadowing still overestimates the risk due to several conservative assumptions. This paper proposes mathematical modifications to the calculation of shadowing to address the risk overestimation. To validate the proposed method, 10^6 sets of aircraft trajectories are generated so that the actual risk can be estimated by counting the number of collisions. The result shows that the risk calculated by the proposed method is much closer to the actual risk compared to the one calculated by the current CRM. The proposed model will help introduce ILS approach at obstacles-sensitive airports.

INDEX TERMS Collision risk model, aircraft navigation, approach, landing, safety.

I. INTRODUCTION

Aircraft landing phase is the most critical phase of each flight and that is why about half of the accidents occur during this phase [1]. Landing is difficult or sometimes impossible under low visibility condition. The Instrument Landing System (ILS) was introduced to partly solve the problem. ILS is a ground system which provides lateral and vertical guidance by sending radio waves to landing aircraft. The aircraft follows a straight fixed-path descent path guided by ILS, and the aircraft can land safely regardless of visibility by following this guidance. Although ILS guidance is very accurate, an aircraft can still deviate from the nominal path due to its navigation error, wind disturbances, etc., and could collide to ground obstacles. Therefore, risk assessment for collision to ground obstacles is mandated for safe operations.

The risk assessment is important in aviation field, with numerous research efforts being made for accurate estimation. The first collision risk model was proposed by Reich [2], [3]. This model calculates the risk for mid-air collision, i.e. collision of two aircraft in flight. This model is stationary, i.e. probability density functions of several flight parameters are assumed to be independent of time, and the collision probability is calculated. Since this model is simple and allows an easy extension, its updated version is still used for the risk assessment of vertical separation standard [4] and lateral separation standard [5]. Later, a time-dependent model was first developed by Hsu [6]. Since the time-dependent model can consider more detailed dynamics of aircraft, it can estimate the collision probability more accurately. The current safety assessment of longitudinal separation standard is conducted based on Hsu model [5]. The minor modifications to Hsu model have been made to represent the flight scenarios/situations considered [7], e.g. application to time-based separation standard [8], [9], lateral/longitudinal separation standard [10], [11], extension of Reich model [12], and application to unmanned aircraft [13]. In addition, there are many parameters which significantly affect the calculated collision probability, so data analysis of actual flight is also important and has been conducted [14], [15].

On the other hand, the safety assessment between aircraft and ground obstacles has taken a different direction. The risk of collision is not numerically calculated, and the protection area where the ground obstacles are not permitted is determined based on navigation specification of aircraft and ground instruments. The exception is the ILS approach. The collision risk model (CRM) to calculate the risk of collision to ground obstacles during ILS approach was developed by

The associate editor coordinating the review of this manuscript and approving it for publication was Haluk Eren.

ICAO in 1970s [16]. The maximum tolerable collision probability per approach (collision probability) to ground obstacles is set to 10^{-7} [17], and this CRM has been used so far and has not been updated since then. There are some researches to reduce the obstacle limitation area [18]–[20], but all of them try to change the latera/vertical distribution, and no effort has been made to improve the core algorithm of CRM calculation itself.

From a safety perspective, the CRM should estimate the risk conservatively, i.e. it should not underestimate the risk. However, too much overestimation of the risk might hinder the introduction of an ILS procedure despite the necessary safety condition being actually met. To the best of the authors' knowledge, no research has been made on how conservatively the current CRM estimates the collision probability numerically. The authors found that significant overestimation in the current CRM is observed when multiple obstacles are in close proximity to one another. This problem has not been identified yet, and the calculation method is worth improving because of the significance of the overestimation in the current CRM.

Therefore, this paper proposes a new calculation method to estimate the collision probability more accurately when there are multiple obstacles located closely to each other. First, the existing CRM (current CRM) is reviewed, with a detailed explanation of the calculation method in Sec. II. Next, a new calculation method is proposed and explained in Sec. III. In Sec. IV, the data sets of landing trajectory are prepared for the validation purpose, and the parameters and distribution functions are estimated from the data. The calculation results are shown in Sec. V, and this paper is summarized in Sec. VI.

II. CURRENT COLLISION RISK MODEL

A. COLLISION RISK MODEL BASICS

The details of the current CRM are described in ICAO document [16]. To aid the reader's understanding of the method, here CRM's calculation flow is explained briefly. The current CRM can calculate the collision probability to hit ground obstacles during approach and missed approach phases. An aircraft is assumed to conduct a missed approach when it reaches the decision height (DH). Therefore, the CRM does not account for the collision when the aircraft proceeds towards landing after reaching DH. The obstacle protection of the flight below DH is provided by another criteria (obstacle free zone [21]). The calculation starts when the aircraft reaches 1000 ft for landing and finishes when the aircraft passes 1000 ft for missed approach. This paper focuses on the approach phase only.

As for the calculation, the aircraft is assumed to be a box, and the collision probability is calculated based on the predetermined distribution of lateral/vertical deviation of aircraft c.g. position, $P_y(x, y)$ and $P_z(x, z)$. Here, x-axis is defined as along-track direction, and y-axis is defined as cross-track direction, and z-axis indicates the vertical (altitude) direction. (0, 0, 0) is located at the threshold. The aircraft width is assumed to be λ_y, and the vertical distance between aircraft c.g. position and the wheel is assumed to be λ_z. A single spike obstacle at $x = x_0$, $y = y_0$ and its height z_0 is given, and the probability to hit this obstacle is calculated by the following form.

$$P = \int_{y_0-\lambda_y/2}^{y_0+\lambda_y/2} P_y(x_0, y)dy \int_0^{z_0+\lambda_z} P_z(x_0, z)dz \qquad (1)$$

Note that lateral and vertical movements are assumed to be independent. Since it is difficult to make a continuous along-track distribution, the vertical and lateral distributions are defined at $x = -7800$ m, -4200 m, and -1200 m, and interpolated exponentially between these points. The distribution function is determined based on the empirical data obtained in 1970s. Deviation is defined in DDM (difference in depth of modulation: linear to localizer/glideslope dot), so the distribution is shrunk or expanded based on the ILS parameters (e.g. localizer/glideslope antenna position, runway length, glideslope angle, reference altitude at threshold). In addition, aircraft size also affects the collision probability, because the size of aircraft box is changed.

Obstacles are modeled as a collection of ''spikes'' and/or ''walls'' depending on their shape. Neither a spike nor a wall is assumed to have any along-track depth. Therefore, multiple spikes or walls should be used to model an obstacle with along-track depth.

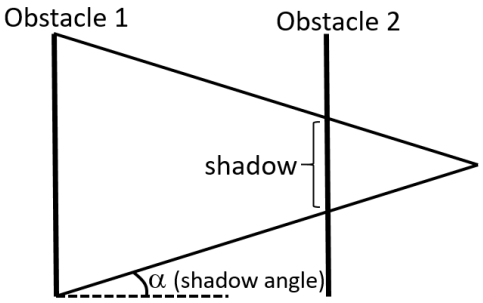

FIGURE 1. Lateral shadowing of Obstacle 1 cast on Obstacle 2.

B. SHADOWING

Once the distributions of lateral and vertical deviation are determined, it is easy to calculate the collision probability with a single obstacle. Multiple obstacles, however, present more difficulties, because the unit of the risk of collision is the number of accidents per approach. If two obstacles are sufficiently separated by each other, the total risk is the summation of the collision probability to individual obstacles. However, if multiple obstacles are located closely together, a simple summation will overestimate the risk because the aircraft is likely to hit the downstream obstacle if it hits an upstream obstacle. This is called double-counting here, and this double-counting causes the risk overestimation.

To avoid overestimation, a shadowing technique is used in the current CRM. Fig. 1 illustrates the shadowing concept. The shadow in the figure shows the part of the obstacle which

will be hit if another upstream obstacle is hit. In other words, the shadow area is equivalent to the area where the risk is already accounted for by the upstream obstacle, so the risk can be estimated more accurately by subtracting the risk of the shadow area from the sum of the risk for all obstacles. To implement shadowing in the calculation, the shadow angle α is set, and the possible double counting area is set as "shadow" as shown in the figure. The shadow angle physically translates to the aircraft deviation angle at the time of hitting the upstream obstacle. In this example, total collision probability R_{all}, can be calculated by the following formula.

$$R_{all} = R_1 + R_2 - R_{shadow,1,2} \tag{2}$$

where R_i is the probability where the aircraft hits the obstacle i, and $R_{shadow,i,j}$ indicates the probability where the aircraft hits both obstacles i and j calculated by shadowing. Although this equation includes two obstacles only, the same calculation method can be easily extended to more obstacles by iteratively calculating the collision probability from upstream to downstream.

This example shows the lateral shadowing only, but the same shadowing can be applied vertically, too. In the current CRM, the lateral shadow angle is set to 14 deg, while the vertical shadow angle is set to (glideslope angle) +0.5 deg.

III. PROPOSED IMPROVEMENT IN CALCULATIONS

A. PROBLEMS IN SHADOWING

Shadowing is a useful technique to avoid the overestimation of risk. The key parameter is the shadow angle. A large shadowing angle causes conservative risk estimation, i.e. overestimation of the risk. On the other hand, the underestimation of the risk should be avoided, so too low shadow angle is not adequate. In the current CRM, a large single shadow angle (14 deg) is used, but the authors argue that a variable shadow angle depending on the situation can reduce the estimated collision probability without underestimating it.

The shadow angle in the current CRM mathematically corresponds to the maximum deviation angle at the time of hitting the upstream obstacle. If the actual deviation angle is smaller than the shadow angle, the shadow area is smaller than the area where the actual aircraft flies over, which leads to the overestimation of the risk. Therefore in this paper, the shadowing calculation is modified to avoid the overestimation of the risk.

B. SUMMARY OF THE PROPOSALS

The authors propose two ways to determine the shadow angle dynamically depending on the situation. Both methods reduce the shadow angle while avoiding the underestimation of the risk, which means that more accurate (smaller) risk of collision can be estimated.

First, percentile values are considered instead of considering the worst case. The proposed algorithm considers several probability ranges, in each of which the worst case is assumed and the collision probability is calculated.

Second, the shadow angle is determined dynamically depending on the deviation magnitude. The aircraft track angle is expected to depend on the deviation magnitude, which is considered in the calculation.

Both methods can be applied simultaneously, and these methods simply replaces the applied shadow angle instead of the fixed value (14 deg). Therefore, the proposed method is expected to show the lower collision probability but greater than the actual collision probability without increasing the computational cost.

C. PROPOSAL 1) MULTIPLE SHADOW ANGLES

To avoid the overestimation of the risk, the authors propose that multiple shadow angles should be assumed. If a single constant shadow angle is set, the maximum deviation angle observed among all data might be appropriate to avoid the underestimation. However, the maximum deviation angle is rarely observed, so multiple shadow angles can potentially reduce the overestimation. $CR(\alpha)$ indicates the calculated collision probability using a single constant shadow angle α. The proposed method to calculate the collision probability is shown in the following form.

$$\sum_{i=1}^{n} (P_{i-1} - P_i) CR(\alpha_i) \quad \forall i,\ \alpha_{i-1} < \alpha_i \& P_{i-1} > P_i \tag{3}$$

where P_i indicates the probability where the actual shadow angle is greater than α_i. $P_0 = 1$ and $P_n = 0$. When $n = 1$, and $\alpha_1 = 14$ deg, the proposed CRM is equivalent to the current CRM. In this expression, the estimation of α_i is important once P_i is determined. If data are available, α_i can be obtained considering the ratio of flight where the maximum deviation angle of a single flight is within the designated range of the probability.

D. PROPOSAL 2) DEPENDENCY OF SHADOW ANGLE ON DEVIATION MAGNITUDE

In the previous subsection, shadow angle was assumed to be constant over the entire flight. In this subsection, the authors argue that the shadow angle can vary depending on the deviation magnitude. In most cases, the aircraft fly along the route with small deviations and small deviation angles. On the other hand, when large deviation is observed, large deviation angle is also needed, so such a large deviation angle is more frequently observed. Although the collision usually occurs when the aircraft deviates from the route, simultaneous large deviations in both lateral and vertical dimensions are extremely rare because CRM assumes independent lateral and vertical deviation distribution. Therefore, when the collision occurs due to a large vertical deviation, the aircraft will probably be still around the route laterally and in such a case the lateral shadow angle should be small to avoid the overestimation.

Here, lateral shadow angle is considered. To hit a ground obstacle (spike) located at $y = y_0$, the aircraft should be at $y = \left[y_0 - \lambda_y/2 \ \ y_0 + \lambda_y/2 \right]$. Once the probability density of lateral deviation and the expected shadow angle at y-position

are determined, the average (expected) shadow angle to hit this obstacle can be calculated as the following expression.

$$\alpha_{ave} = \int_{y_0-\lambda_y/2}^{y_0+\lambda_y/2} \alpha_y P_y(y) dy \Bigg/ \int_{y_0-\lambda_y/2}^{y_0+\lambda_y/2} P_y(y) dy \qquad (4)$$

where $P_y(y)$ is the probability density of lateral deviation, and α_y is the expected shadow angle at y. From a safety perspective, the worst shadow angle should be used. However, the lateral distribution is exponentially decreased with y-position, and it is extremely rare to observe the worst shadow angle. Therefore, the average of shadow angle is expected to be a good approximation.

In the current CRM, the shadow angle is constant through the calculation. However, this method applies a different deviation angle depending on the position of the obstacle. This method can also be used simultaneously with the proposed method in subsection III B. The proposed calculation is given by the following equation.

$$\sum_{i=1}^{n} (P_{i-1} - P_i) CR_{new}(\alpha_{i,1}, \alpha_{i,2}, \ldots, \alpha_{i,m}) \qquad (5)$$

CR_{new} is the calculated collision probability with different shadow angles $\alpha_{i,1}, \alpha_{i,2}, \ldots, \alpha_{i,m}$. The shadow angle of $\alpha_{i,j}$ means the expected shadow angle in each range of aircraft lateral deviation between d_{j-1} and d_j, and is given as tabular data. The shadow angle applied is calculated by using $\alpha_{i,j}$ depending on the lateral obstacle position as shown in Eq. (5).

IV. DATA PREPARATION

A. TRAJECTORY DATA USED

In order to verify the effectiveness of the methods proposed in the previous section, trajectory data sets are needed. Here, landing trajectories are generated via numerical simulations. The author has developed a pilot control model to conduct a landing simulation in the past research [22], and using this model, 10^6 times simulations are conducted with different flight conditions. The FAA random wind model for evaluation [23] is used, and the simulation starts at trimmed condition. The initial lateral position is uniformly distributed between -0.25 dot and 0.25 dot for localizer, and the vertical distribution is between -0.5 dot and 0.5 dot for glideslope. Finally, 10^6 sets of trajectory data are obtained.

Based on the obtained trajectory, empirical lateral and vertical distributions are obtained. The probability density function is modeled with the empirical distribution, and is used to calculate the collision probability. The shadowing parameters used in the proposed methods (P_i, d_j, $\alpha_{i,j}$) are also obtained from the data sets. The actual collision probability can be obtained by counting the number of collisions divided by the number of trajectories (10^6). This method is called ''counting'' here, and this value is assumed to be the actual collision probability, which is used to compare the collision probability calculated by the current CRM and the proposed method for the validation purpose. In counting the number of collision, the time series of trajectory data is linearly interpolated, and the collision is counted if any of the interpolated trajectory goes through the obstacles.

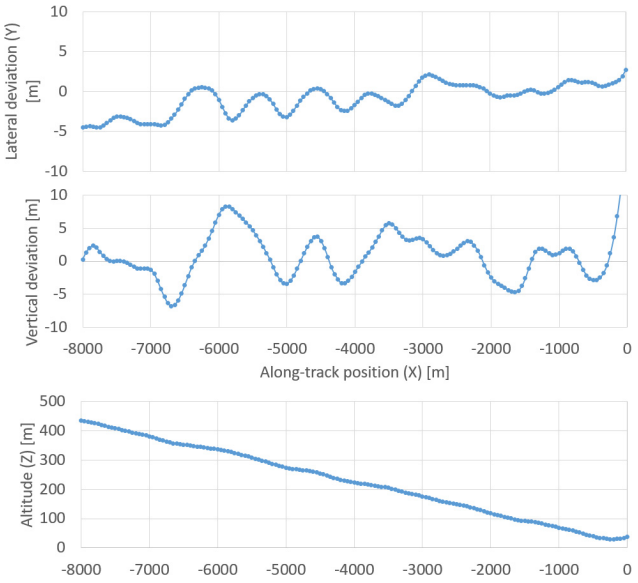

FIGURE 2. Example of trajectory.

The purpose of this paper is to verify the proposed calculation method, and not to estimate the collision probability in the real world (i.e. accurate estimation of the lateral/vertical distributions). Real data verification could increase the fidelity of the research. . However, the CRM should estimate the collision probability of the order of 10^{-7}, and sufficient data sets (at least the order of 10^5 or 10^6) are required to validate the proposed calculation method from a statistical viewpoint. However, it is almost impossible to obtain such number of data sets in the real world. In addition, the obtained trajectories are investigated by some retired airline pilots, and it is confirmed that the simulated trajectory is reasonable and not far from the actual trajectory. Therefore, simulation data are used for the validation of the proposed model.

Fig. 2 shows data sample trajectory. In this case, the aircraft flies along the route within 5 m errors in lateral dimension and within 9 m in vertical dimension. The aircraft starts missed approach and starts climbing around $x = -500$ m.

Fig. 3 shows an example of the trajectory data when a large deviation is observed. The maximum lateral deviation here is 60 m. Although there are few data like this example, they strongly affect the collision probability because these data strongly affect the tail of the distribution.

In this simulation, the expected touchdown point is $x = 284.7$ m, and decision height is set to 60 m. Therefore, the aircraft is expected to conduct a missed approach at $x = -860.2$ m. The CRM assumes the collision below 300 m only, which corresponds to $x = -5439.7$ m.

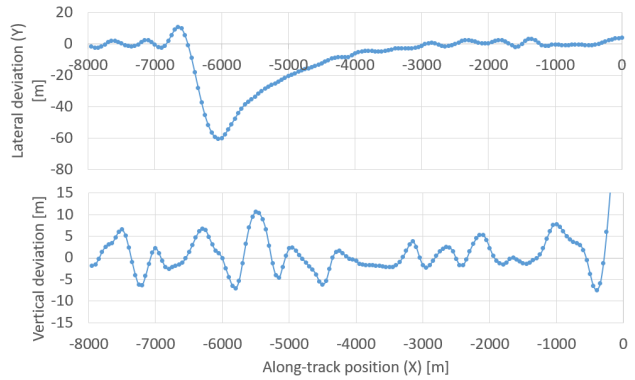

FIGURE 3. Example of trajectory with large lateral deviation.

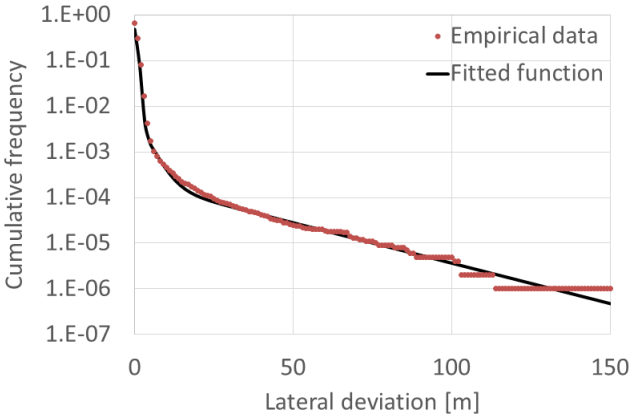

FIGURE 4. Cumulative distribution function of empirical data and fitted distribution function in lateral dimension at x = −4200 m.

B. DISTRIBUTION FUNCTIONS

Fig. 4 and Fig. 5 show the cumulative distribution of generated trajectory data and the modeled distribution function at $x = -4200$ m in lateral and vertical domains. This time, the lateral distribution is modeled by the combination of Johnson SU and Laplace distribution, and the vertical distribution is modeled by Johnson SU distribution. Probability density functions of Johnson SU distribution and Laplace distribution are given as follows:

$$J(x;\gamma,\xi,\delta,\lambda) = \frac{\delta}{\lambda\sqrt{2\pi}} \frac{1}{\sqrt{1+\left(\frac{x-\xi}{\lambda}\right)^2}} \times \exp\left(-\frac{1}{2}\left(\gamma+\delta\sinh^{-1}\left(\frac{x-\xi}{\lambda}\right)\right)^2\right) \tag{6}$$

$$L(x;\lambda,\mu) = \frac{1}{2\lambda}\exp\left(-\frac{|x-\mu|}{\lambda}\right) \tag{7}$$

Although there is a small discrepancy between the empirical data and distribution data in both dimensions, the distribution function in general fits the empirical data. Similar distribution functions are generated in the same way

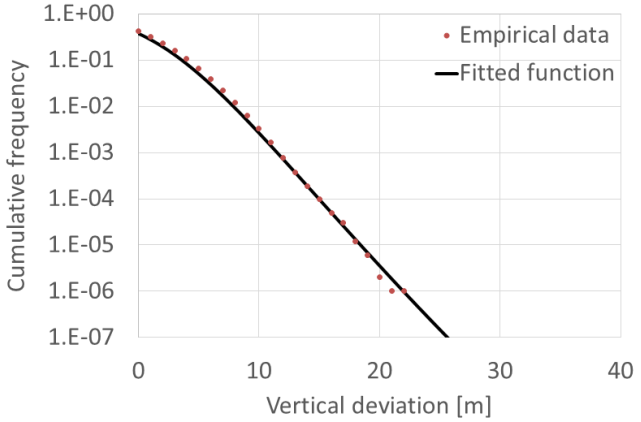

FIGURE 5. Cumulative distribution function of empirical data and fitted distribution function in vertical dimension at x = −4200 m.

at $x = -7800$ m and -1200 m, and these functions are used to calculate the collision probability with current CRM and the proposed CRM.

C. ESTIMATION OF THE VARIABLE SHADOW ANGLES

In this paper, the multiple shadow angles with different probabilities are assumed, and the shadow angle is changed depending on the deviation magnitude.

Based on (4), P_i, d_j, and $\alpha_{i,j}$ should be defined. First, the following P_i and d_j are chosen.

$$d_j = \{0, 3, 6, 9, 12, 15, 9999\} \tag{8}$$

$$P_i = \{1, 0.9, 0.8, 0.7, 0.6, 0.5, 0.4, 0.3, 0.2, 0.1, 0.01, 0.001, 10^{-4}, 10^{-5}, 0\} \tag{9}$$

Since higher accuracy is obtained if P_i and d_j are finely divided. This time, especially P_i is divided finely in this calculation. $\alpha_{i,j}$ indicates the shadow angle applied in each condition. This value is obtained based on the simulated trajectory data. First, data is used only where x position is between -5439.7 m and -860.2 m. Next, pick up the flight where there is at least one data when the deviation is between d_{j-1} and d_j. The maximum shadow angle when the deviation is within d_j for each trajectory is calculated (=calculated shadow angle). The value of $\alpha_{i,j}$ is simply estimated by the 100(1–P_i) percentile of the calculated shadow angle when P_i is large. When P_i is small, it is difficult to estimate the corresponding calculated shadow angle by the percentile method because limited number of trajectories are available. Therefore, the peak over threshold (POT) method is applied.

POT method [24] is one of extreme value statistics used in estimating the frequency of occurrence exceeding thresholds. In POT, the probability variables exceeding thresholds are assumed to follow generalized Pareto distributions, whose cumulative distribution function is given as follows:

$$H(y) = 1 - \left(1+\xi\frac{y}{\sigma}\right)^{-1/\xi}, \quad 1+\xi y/\sigma > 0 \tag{10}$$

A threshold should be determined in POT before the parameter values ξ and σ are estimated. The threshold is

TABLE 1. Shadow angle $\alpha_{i,j}$ in each P_i and d_j.

P_i / d_j	3	6	9	12	15	9999
0.9	0.446	0.649	1.262	1.942	2.352	2.976
0.8	0.514	0.745	1.504	2.448	3.059	3.621
0.7	0.570	0.820	1.741	2.804	3.456	4.085
0.6	0.624	0.888	1.982	3.111	3.818	4.543
0.5	0.679	0.955	2.249	3.444	4.242	4.964
0.4	0.739	1.029	2.561	3.835	4.729	5.452
0.3	0.811	1.117	2.965	4.420	5.267	5.935
0.2	0.906	1.236	3.597	5.135	5.938	**6.592**
0.1	1.066	1.460	4.831	**6.182**	**6.912**	**7.712**
0.01	1.889	3.666	**7.684**	**9.002**	**9.782**	**11.57**
0.001	4.603	**6.711**	**9.916**	**11.40**	**12.17**	**15.64**
0.0001	**7.158**	**8.943**	**11.73**	**13.43**	**14.15**	**19.95**
0.00001	**9.233**	**10.73**	**13.19**	**15.15**	**15.80**	**24.50**
0	90	90	90	90	90	90

determined so that the parameter values ξ and σ are stabilized near the threshold. Finally the distribution of $\alpha_{i,j}$ is obtained as shown in Table 1. The bold values in the table are estimated based on the generalized Pareto distribution models. As the lateral deviation becomes larger, the corresponding shadow angle becomes also larger. Even when the lateral deviation is small ($d_j = 3$), large shadow angle (more than 9 deg) is observed with very low probability.

The above Table 1 always assumes a positive shadow angle. However, at the time of collision, the aircraft does not necessarily fly toward the obstacle. If the aircraft flies against the obstacle, the aircraft will never hit the adjacent downstream obstacle, which means that the shadow angle can be assumed to be zero. Since the selection of the shadow angle affects the collision probability especially when the aircraft flies against the centerline, zero shadow angle is assumed with a certain probability when the shadow is made against the centerline. When the shadow is made toward the centerline, the values in Table 1 are used, which is a conservative estimation. To calculate the probability of a zero shadow angle, the following data is obtained. First, pick up the data where the aircraft is flying toward the centerline. Next, the number of data not deviating further than the initial position for the next 1000 m flight is counted as shown in Fig. 6. Zero shadow angle is assumed when both of the following conditions are met.

a) The aircraft is not going against the centerline at considered obstacle. (obstacle 1 in figure)
b) The aircraft is not going beyond the initial position laterally within 1000 m flight (up to hitting obstacle 2 in figure).

The obtained number is divided by the total data point, which is the probability that zero shadow angle can be assumed. Table 2 summarizes the result in each range of initial lateral deviation. When the initial deviation is small (0-3 m), most aircraft flies back to the initial lateral position. However, as the initial lateral deviation increases, less aircraft will come back to the initial lateral position. That is because

TABLE 2. Zero shadow angle probability in each range of initial lateral deviation.

0-3	3-6	6-9	9-12	12-15	15-
0.214	0.522	0.572	0.628	0.658	0.688

TABLE 3. Shadow angle $\alpha_{i,j}$ in each P_i and d_j when the shadow is made against the centerline.

P_i / d_j	3	6	9	12	15	9999
0.9	0	0	0	0	0	0
0.8	0	0	0	0	0	0
0.7	0.454	0	0	0	0	0
0.6	0.535	0	0	0	0	0
0.5	0.605	0	0	0	0	0
0.4	0.674	0.714	1.156	0	0	0
0.3	0.751	0.869	1.739	2.420	2.593	2.131
0.2	0.851	1.015	2.341	3.303	3.884	4.342
0.1	1.011	1.223	3.350	4.632	5.310	5.844
0.01	1.736	2.635	**6.737**	**7.847**	**8.511**	**9.590**
0.001	4.247	**5.884**	**9.147**	**10.42**	**11.11**	**13.55**
0.0001	**6.918**	**8.281**	**11.10**	**12.60**	**13.27**	**17.74**
0.00001	**9.033**	**10.20**	**12.69**	**14.45**	**15.07**	**22.16**
0	90	90	90	90	90	90

of the lateral deviation trend as shown in Fig. 3. When the large lateral deviation is observed, the aircraft rapidly deviates to the maximum lateral deviation position, and goes back to the centerline gradually. This means that the aircraft is more likely to fly toward the centerline when the initial deviation is large. Assuming the probability to apply zero shadow angle as shown in Table 2, a new shadow angle table can be created for the case when the shadow is made against the centerline as shown in Table 3. The shadow angle table of either Table 1 or Table 3 is used depending on the direction of shadow made. When the shadow is made against the centerline and two obstacles are separated within 1000 m, Table 3 is used. Otherwise, Table 1 (more conservative shadow angle) is used.

D. ASSUMED GROUND OBSTACLES

To calculate the collision probability, the positioning of ground obstacles is also important. All obstacles in CRM are assumed to be a wall or a spike, so a single wall can be described by 4 coordinates (x-position, y-position (left), y-position (right), z-position), because the bottom of the wall is assumed to be $z = 0$.

Therefore, the wall constructed by the following coordinates can be expressed as (−4500, 50, 100, 1000).

Coordinates: (−4500, 50, 0)
(−4500, 50, 1000)
(−4500, 100, 1000)
(−4500, 100, 0)

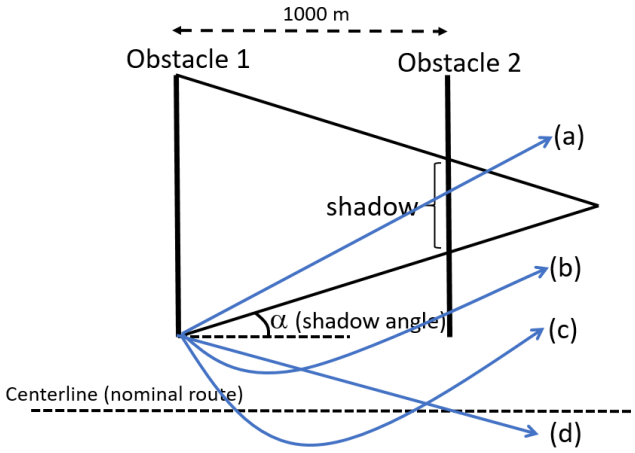

FIGURE 6. Several cases whether the shadow angle can be assumed to be zero. (a), the aircraft is going against the centerline, so zero shadow angle cannot be assumed. (b), the aircraft is going toward the centerline at the beginning, but the aircraft goes beyond the initial lateral deviation again within 1000 m, so zero shadow angle cannot be assumed. (c) and (d), the aircraft is going toward the centerline, and the aircraft does not go back to the initial lateral deviation within 1000 m, so zero shadow angle can be assumed.

Note that a spike can be also described as a wall if y-position (left) is equal to y-position (right).

This time, to confirm the effectiveness of the proposed CRM, the following obstacles are assumed.

(a) Obstacle A (1 wall)
(−3000, 50, 100, 1000)
(b) Obstacle A-101 (101 walls)
For i = 0 to 100
(−3000+*i*, 50, 100, 1000)
(c) Obstacle A-11 (11 walls)
For i = 0 to 10
(−3000 + 10*i, 50, 100, 1000)
(d) Obstacle A-2 (2 walls)
(−3000, 50, 100, 1000)
(−2900, 50, 100, 1000)
(e) Obstacle B (1 wall)
(−1500, −100, −60, 1000)
(f) Obstacle B-101 (101 walls)
For i = 0 to 100
(−1500 + i, −100, −60, 1000)
(g) Obstacle B-11 (11 walls)
For i = 0 to 10
(−1500 + 10*i, −100, −60, 1000)
(h) Obstacle B-2 (2 walls)
(−1500, −100, −60, 1000)
(−1400, −100, −60, 1000)
(i) Obstacle C (1 spike)
(−2500, −30, −30, 123)
(j) Obstacle C-101 (101 spikes)
For i = 0 to 100
(−2500 + i, −30, −30, 123 − i ∗ tan(3 deg))
(k) Obstacle C-11 (11 spikes)

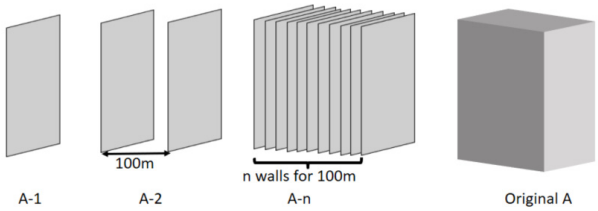

FIGURE 7. Schematic image of obstacle A.

For i = 0 to 10
(−2500 + 10*i, −30, −30, 123 − 10*i ∗ tan(3 deg))
(l) Obstacle C-2 (2 spikes)
(−2500, −30, −30, 123)
(−2400, −30, −30, 117)
(m) Obstacle D (1 wall)
(−4000, 35, 100, 210)
(n) Obstacle D-101 (101 walls)
For i = 0 to 100
(−4000 + i, 35, 100, 210 − i ∗ tan(3 deg))
(o) Obstacle D-11 (11 walls)
For i = 0 to 10
(−4000 + 10*i, 35, 100, 210 − 10*i* tan(3 deg))
(p) Obstacle D-2 (2 walls)
(−4000, 35, 100, 210)
(−3900, 35, 100, 204)
(q) Obstacle E (2 walls)
(−4500, 37, 100, 200)
(−4400, 37, 100, 200)

Obstacle A is a single wall, whereas Obstacle A-101, A-11, and A-2 model the same rectangular cuboid obstacle. Since all obstacles must consist of walls in the calculation, a rectangular cuboid obstacle should be modeled as several walls. The difference of obstacles A-101, A-11 and A-2 is found in the number of assumed walls. If the number of walls increases, it is likely to cause overestimation of the risk because of double-counting. On the other hand, less walls can cause underestimation of the risk because of the sparse modeling of the obstacle. Also, for a better understanding of the obstacles, the schematic image of obstacle A is shown in Fig. 7. Obstacle B is similarly modeled like Obstacle A at a different position.

Obstacle C is a single spike, and Obstacles C-101, C-11, and C-2 indicate the same obstacle but the assumed number of spikes is different. This obstacle is not a rectangular, but the ceiling is lowered with a glide slope angle (3 deg). Obstacle D is also similarly modeled like Obstacle C at a different position.

Appendix is devoted to the explanation of the proposed shadowing method, and Obstacle E is used only as an example in the explanation.

V. CALCULATION RESULTS

A. COLLISION PROBABILITY WITH A SINGLE OBSTACLE

First, the collision probability with a single obstacle is considered. When there is only one obstacle, double counting does

TABLE 4. Collision probability to a single obstacle calculated by various methods.

Obstacles	A	B	C	D
Current CRM	4.96E–5	4.19E–5	1.77E–5	1.46E–5
Proposed CRM	4.96E–5	4.19E–5	1.77E–5	1.46E–5
Counting	5.00E–5	3.30E–5	1.90E–5	1.30E–5

not occur and no shadowing is needed. Therefore, the calculated collision probability by current/proposed CRM and counting should almost match. Table 4 shows the result of the calculation. Obstacles A, B, C, and D are used for the calculation. The only difference of the current CRM and the proposed CRM is the shadow angle, so the estimated collision probability exactly match between them. According to the result, the collision probabilities by counting and both CRMs are almost the same. There is small difference between counting and CRMs because of the discrepancy of the distribution model with the empirical distribution illustrated in Fig. 4 and Fig. 5. This result shows that the collision probability is well estimated by both current and proposed CRM, and the lateral and vertical probability density functions used in the calculation are appropriate.

B. COLLISION PROBABILITY WITH MULTIPLE OBSTACLES

Next, the collision probability with multiple obstacles is considered. The relative risk to a single obstacle is shown in Table 5. Since there is small discrepancy between the result by CRM and counting even when a single obstacle is assumed as shown in Table 4, the relative risk (collision probability to multiple obstacles / collision probability to a single obstacle) is more appropriate for the comparison purpose. Since the multiple obstacles should always give a greater risk than the single obstacle, the relative risk should always be greater than 1. The collision probabilities by CRMs are expected to be close to the one by counting.

First, obstacles A-101, A-11, and A-2 are considered, all of which model the same rectangular cuboid obstacle. Using the counting, the calculated collision probabilities among A-101, A-11 and A-2 are the same in this example. Compared to the obstacle A (single obstacle), the collision probability increases by 1.220 times only. Less walls can cause the underestimation of the risk, but this case, the impact of the number of walls on the collision risk seems to be small. On the other hand, using the current CRM, the collision probability becomes larger when more walls are assumed. The collision probability with obstacle A-101 is 4.652 times larger than that with obstacle A, while it is actually 1.220. Using the proposed CRM, however, the difference of the collision probability among number of obstacles is small, which is the same trend as counting. Even with obstacle A-101, the collision probability is 1.574 times larger than that with obstacle A. This result is slightly greater than the actual value (1.220), but much less than that calculated by the current CRM (4.652). The similar trend is observed in obstacle B-101, B-11, and B-2.

TABLE 5. Relative collision probability to multiple obstacles to single obstacle calculated by various methods.

	A-101	A-11	A-2
Current CRM	4.652	3.937	1.869
Proposed CRM	1.574	1.517	1.246
Counting	1.220	1.220	1.220

	B-101	B-11	B-2
Current CRM	2.628	2.389	1.675
Proposed CRM	1.255	1.233	1.149
Counting	1.091	1.091	1.091

	C-101	C-11	C-2
Current CRM	12.657	6.027	1.581
Proposed CRM	2.222	1.769	1.261
Counting	1.632	1.421	1.316

	D-101	D-11	D-2
Current CRM	19.340	9.437	8.529
Proposed CRM	3.827	2.932	1.827
Counting	1.923	1.767	1.462

Next, obstacles C-101, C-11, and C-2 are considered. The y-position of these obstacles is −30 m, so the possible aircraft position is [−60, 0]. Therefore, the small shadow angle depending on the deviation magnitude as explained in Section III C will suffice. However, the vertical shadow is also considered in this example. Using the counting, the collision probability gradually increases with the assumed number of walls, the collision probability with obstacle C-101 is 1.581 times larger than that with obstacle C. Using the current CRM, the collision probability sharply increases with the assumed number of walls, and the collision probability with obstacle C-101 is 12.657 times larger than that with obstacle C, while it is actually only 1.632. This seems to be due to too large a shadow angle is applied regardless of the aircraft lateral position. On the other hand, using the proposed CRM, the collision probability gradually increases with the assumed number of walls, and the collision probability with obstacle C-101 is 2.222 times larger than that with obstacle C. Although this value is larger than the actual counting value (1.581), it is much smaller than that the current CRM (12.657). In the same way, as for obstacles D-101, D-11, and D-2, the proposed CRM shows much smaller collision probability than that calculated by the current CRM.

The advantage of the proposed model is more significant for obstacles C and D than obstacles A and B. Obstacles A and B are located far from the centerline, which means that the aircraft needs to deviate laterally to hit obstacles C and D. In this situation, the applied shadow angle is always the same if y >= 15m, which means that the effect of the proposal 2) (shadow angle selection depending on the deviation magnitude) is limited. On the other hand, aircraft will obstacle C and D with small lateral deviation (considering the aircraft size, the aircraft will hit the obstacle at y = 0 for obstacle C), so both effects of proposal 1) and 2) work well. Considering

this fact, both methods appropriately work to estimate the collision probability more accurately.

As shown in these results, the proposed CRM can estimate the collision probability more accurately when there are multiple obstacles. In general, there are many reasons that more walls should be used to model the obstacles. 1) The sparse modeling can cause the underestimation of the risk. As shown in Table 5, the collision probability varies with the number of assumed walls even for counting. That means that sparse obstacle modeling could underestimate the risk. 2) The sparse modeling cannot model the complicated shape of the obstacle. If the obstacle has a complicated shape, there are many ways of modeling the obstacle using sparse walls and we should choose one of them subjectively. Using the proposed CRM, the overestimation of the risk is relatively much smaller than that by the current CRM, so the complicated shape of the obstacle can be modeled more accurately with dense walls with avoiding too much over-estimation.

VI. CONCLUSION

This paper proposed a new calculation method to estimate the collision probability under ILS approach when there are multiple ground obstacles. The current CRM uses the mitigation method (shadowing) to reduce the overestimation of the risk, even though it does not eliminate overestimation completely. The proposed CRM varied the shadow angle according to the probability and magnitude of deviation, and it successfully estimated the collision probability more accurately compared to the current CRM. This result will help the introduction of a new ILS procedure by estimating the risk of collision more accurately.

APPENDIX

To illustrate the proposed calculation method, a sample shadow calculation for the case of obstacle E is shown. The aircraft width is assumed to be 60 m.

Consider $i = 7$ (i.e. $P_i = 0.3$). Here, wall1 $(-4500, 37, 50, 200)$ makes a shadow on wall2 $(-4400, 37, 50, 200)$. Since the left edge of wall1 is located at 37 m laterally, the possible aircraft y-position to hit the left edge is [7, 67]. According to Eq. (4), the expected shadow angle to hit the left edge of wall1 is calculated in the following way:

$$\alpha_{left} = \int_7^{67} \alpha_y P_y(y)dy \Big/ \int_7^{67} P_y(y)dy \tag{11}$$

α_y is chosen from Table 3 because the shadow is made against the centerline. $P_y(y)$ is obtained in Sec. IV B. Eq. (11) is actually calculated in the following way.

$$\begin{aligned}\alpha_{left} &= \Big(\int_7^9 1.739P_y(y)dy + \int_9^{12} 2.420P_y(y)dy \\ &\quad + \int_{12}^{15} 2.593P_y(y)dy \\ &\quad + \int_{15}^{67} 2.131P_y(y)dy\Big) \Big/ \int_7^{67} P_y(y)dy \\ &= 2.009\end{aligned} \tag{12}$$

In the same way, the possible aircraft y-position to hit the right edge is [70, 130]. The expected shadow angle to hit the right edge of wall1 is calculated in the following way:

$$\alpha_{right} = \int_{70}^{130} \alpha_y P_y(y)dy \Big/ \int_{70}^{130} P_y(y)dy = 5.935 \tag{13}$$

α_y is chosen from Table 1 because the shadow is made toward the centerline. The calculated shadow angle at left and right edge of wall1 is 2.009 deg and 5.935 deg, respectively.

The vertical shadow is always assumed to be 3.5 deg. Finally, the shadow wall on wall2 can be expressed as the following wall.

$(-4400, 37 + 100^* \tan(2.009\,\text{deg}), 100 - 100^* \tan(5.935\,\text{deg}), 200 - 100^* \tan(3.5\,\text{deg})) = (-4400, 40.508, 89.604, 193.884)$

The collision probability of wall1, wall2, and calculated shadow wall are calculated. This calculation is repeated in various i (probabilities), and the total risk is calculated by Eq. (5).

REFERENCES

[1] *Statistical Summary of Commercial Jet Airplane Accidents*, Boeing, Chicago, IL, USA, 2017.
[2] P. G. Reich, "Analysis of long-range air traffic systems: Separation standards—I," *J. Navigat.*, vol. 19, no. 1, pp. 88–98, Jan. 1966, doi: 10.1017/S037346330004056X.
[3] P. G. Reich, "Analysis of long-range air traffic systems: Separation standards—III," *J. Navigat.*, vol. 19, no. 3, pp. 331–347, Jul. 1966, doi: 10.1017/S0373463300047445.
[4] *Operating Procedures and Practices for Regional Monitoring Agencies in Relation to the Use of a 300 m (1000 ft) Vertical Separation Minimum Between FL 290 and FL 410 Inclusive*, document 9937, Int. Civil Aviation Org., Montreal, QC, Canada, 2010.
[5] *Manual on Monitoring the Application of Performance-Based Horizontal Separation Minima*, document 10063, Int. Civil Aviation Org., Montreal, QC, Canada, 2017.
[6] D. A. Hsu, "The evaluation of aircraft collision probabilities at intersecting air routes," *J. Navigat.*, vol. 34, no. 1, pp. 78–102, Jan. 1981, doi: 10.1017/S0373463300024279.
[7] S. Alam, C. Lokan, G. Aldis, S. Barry, R. Butcher, and H. Abbass, "Systemic identification of airspace collision risk tipping points using an evolutionary multi-objective scenario-based methodology," *Transp. Res. C, Emerg. Technol.*, vol. 35, pp. 57–84, Oct. 2013, doi: 10.1016/j.trc.2013.05.010.
[8] FAA, "Analysis and recommendation of the potential for the reduction of longitudinal separation in pacific ocean environment," Federal Aviation Admin., Washington DC, USA, Tech. Rep. DOT/FAA/CT-TN85/39, 1986.
[9] R. Mori, "Safety assessment for reduced time-based separation minima on oceanic routes," *J. Mech. Syst. Transp. Logistics*, vol. 4, no. 1, pp. 39–49, 2011, doi: 10.1299/jmtl.4.39.
[10] S. Barry, "Manual for ATS surveillance separation using RCP240 communications-'ASEPS' or space-based ADS-B manual," Int. Civil Aviation Org., Montreal, QC, Canada, Tech. Rep. ICAO SASP WG/32, 2019.
[11] R. Mori, "Refined collision risk model for oceanic flight under longitudinal distance-based separation in ADS-C environment," *J. Navigat.*, vol. 67, no. 5, pp. 845–868, Sep. 2014, doi: 10.1017/S0373463314000162.
[12] P. Brooker, "Lateral collision risk in air traffic track systems: A 'post-Reich'event model," *J. Navigat.*, vol. 56, no. 3, pp. 399–409, Sep. 2003, doi: 10.1017/S0373463303002455.
[13] A. McFadyen and T. Martin, "Understanding vertical collision risk and navigation performance for unmanned aircraft," presented at the IEEE/AIAA 37th Digit. Avionics Syst. Conf., 2018.
[14] C. Falk, "Observed aircraft speeds and along track speed prediction errors in oceanic airspace," Int. Civil Aviation Org., Montreal, QC, Canada, Tech. Rep. ICAO SASP WG/23, 2013.
[15] R. Mori, "Analysis of speed prediction error on oceanic flights," *J. Navigat.*, vol. 72, no. 06, pp. 1469–1480, Nov. 2019, doi: 10.1017/S0373463319000432.

[16] *Manual on the Use of Collision Risk Model for ILS Operations*, document 9274, Int. Civil Aviation Org., Montreal, QC, Canada, 1980.
[17] *Procedures for Air Navigation Service—Aircraft Operations (PANS-OPS)*, document 8168, Int. Civil Aviation Org., Montreal, QC, Canada, 2010.
[18] T. Murphy, "GBAS alert limits compared to ILS collision risk model navigation system error assumptions," in *Proc. Nat. Tech. Meeting Inst. Navigat.*, 2006, pp. 327–341.
[19] C. Thiel and H. Fricke, "Collision risk on final approach–a radar-data based evaluation method to assess safety," in *Proc. Int. Conf. Res. Air Transp. (ICRAT)*, 2010, pp. 473–480.
[20] H. Fricke and C. Thiel, "A methodology to assess the safety of aircraft operations when aerodrome obstacle standards cannot be met," in *Proc. 10th USA/Eur. Air Traffic Manage. Res. Develop. Seminar (ATM)*, 2013.
[21] *Annex 14 Aerodromes Volume I Aerodrome Design and Operations*, Int. Civil Aviation Org., Montreal, QC, Canada, 2016.
[22] R. Mori, "Pilot control modeling with stochastic periodical discrete movement," *IEEE Trans. Aerosp. Electron. Syst.*, vol. 54, no. 2, pp. 912–922, Apr. 2018, doi: 10.1109/TAES.2017.2768881.
[23] *Federal Aviation Administration, Criteria for Approval of Category III Weather Minima for Takeoff, Landing, and Rollout*, document AC120-28D, 1999.
[24] S. Coles, *An Introduction to Statistical Modeling of Extreme Values*. London, U.K.: Springer Verlag, 2011.

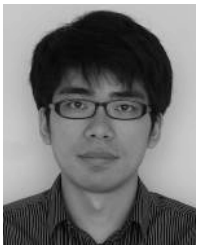

RYOTA MORI was born in Kumamoto, Japan, in 1983. He received the B.S. degree, in 2005, the M.S. degree, in 2007, and the Ph.D. degree in aeronautics and astronautics from The University of Tokyo, in 2010.

He has been with the Air Traffic Management Department, Electronic Navigation Research Institute, Tokyo, Japan, since 2009. His current research includes air traffic management especially for airport traffic optimization and collision risk modeling.

Dr. Mori is a member of the Japan Society for Aeronautical and Space Sciences and the American Institute of Aeronautics and Astronautics.

MASATO FUJITA was born in Hyogo, Japan, in 1975. He received the B.S. degree, in 1998, the M.S. degree, in 2000, and the Ph.D. degree in mathematics from Kyoto University, in 2005.

From 2005 to 2014, he was a Researcher with the Air Traffic Management Department, Electronic Navigation Research Institute. Since 2014, he has been an Associate Professor with the Japan Coast Guard Academy, Hiroshima, Japan. His research interest includes mathematical modeling in air traffic management, such as collision risk modeling and application of machine learning techniques to them.

Dr. Fujita is a member of the Japan Society for Aeronautical and Space Sciences, the American Institute of Aeronautics and Astronautics, the American Mathematical Society, the Mathematical Society of Japan, the Society for Industrial and Applied Mathematics, and the Association for Computing Machinery.